

# Preferred Orientations of Phosphoinositides in Bilayers and Their Implications in Protein Recognition Mechanisms

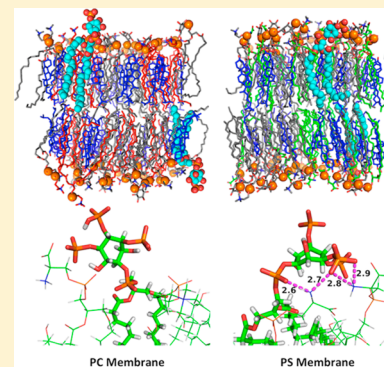
Emilia L. Wu,<sup>†</sup> Yifei Qi,<sup>†</sup> Kevin C. Song,<sup>†</sup> Jeffery B. Klauda,<sup>‡</sup> and Wonpil Im<sup>\*,†</sup>

<sup>†</sup>Department of Molecular Biosciences and Center for Bioinformatics, The University of Kansas, Lawrence, Kansas 66047, United States

<sup>‡</sup>Department of Chemical and Biomolecular Engineering, The University of Maryland, 2113 Chemical and Nuclear Engineering, College Park, Maryland 20742, United States

## Supporting Information

**ABSTRACT:** Phosphoinositides (PIPs), phosphorylated derivatives of phosphatidylinositol (PI), are essential regulatory lipids involved in various cellular processes, including signal transduction, membrane trafficking, and cytoskeletal remodeling. To gain insight into the protein-PIPs recognition process, it is necessary to study the inositol ring orientation (with respect to the membrane) of PIPs with different phosphorylation states. In this study, 8 PIPs (3 PIP, 2 PIP<sub>2</sub>, and 3 PIP<sub>3</sub>) with different phosphorylation and protonation sites have been separately simulated in two mixed bilayers (one with 20% phosphatidylserine (PS) lipids and another with PS lipids switched to phosphatidylcholine (PC) lipids), which roughly correspond to yeast membranes. Uniformity of the bilayer properties including hydrophobic thickness, acyl chain order parameters, and heavy atom density profiles is observed in both PS-contained and PC-enriched membranes due to the same hydrophobic core composition. The relationship between the inositol ring orientation (tilt and rotation angles) and its solvent-accessible surface area indicates that the orientation is mainly determined by its solvation energy. Different PIPs exhibit a clear preference in the inositol ring rotation angle. Surprisingly, a larger proportion of PIPs inositol rings stay closer to the surface of PS-contained membranes compared to PC-enriched ones. Such a difference is rationalized with the formation of more hydrogen bonds between the PS/PI headgroups and the PIPs inositol rings in PS-contained membranes. This hydrogen bond network could be functionally important; thus, the present results can potentially add important and detailed features into the existing protein-PIPs recognition mechanism.



## INTRODUCTION

Phosphoinositides (PIPs), phosphorylated derivatives of phosphatidylinositol (PI), are essential components of eukaryotic cell membranes.<sup>1</sup> The inositol ring hydroxyl groups of PIs can be phosphorylated at the 3, 4, and 5 positions (Figure 1) by specific kinases, giving rise to a group of structurally related PIPs, such as phosphatidylinositol-monophosphate (PI3P, PI4P, and PI5P), phosphatidylinositol-bisphosphate (PI(3,4)P<sub>2</sub>, PI(3,5)P<sub>2</sub>, and PI(4,5)P<sub>2</sub>), and phosphatidylinositol-trisphosphate (PI(3,4,5)P<sub>3</sub>).<sup>2,3</sup> Unlike lipids with common headgroups such as phosphatidylcholine (PC) and phosphatidylserine (PS), PIPs are only present in biological membrane transiently or at low abundance.<sup>2</sup> However, PIPs are indispensable regulatory lipids involved in various cellular processes, including signal transduction, membrane trafficking, and cytoskeletal remodeling.<sup>3,4</sup> For instance, PI4P is crucial for vesicular carrier formation in the trans-Golgi network, and also a protein recruitment control.<sup>3,5,6</sup> PI(4,5)P<sub>2</sub> is responsible for the activation of many ion channels and enzymes, involved in both endocytosis and exocytosis, and is also the source of several second messengers.<sup>7–10</sup>

The cell signaling and regulatory effects of PIPs are mediated by the specific interactions between the characteristic PIPs

headgroups and their target proteins.<sup>2</sup> A number of proteins have been identified to contain a specific PIP-binding motif, such as pleckstrin homology (PH) domains, the Fab1p-YOPB-Vps27p-EEA1 (FYVE) domain, and the Phox homology (PX) domain, indicating that a broad range of cellular processes involves PIPs-binding as part of control mechanisms.<sup>2,7,11</sup> Through the domain recognition of a unique arrangement of phosphate groups around the inositol ring, referred to as a “PI code” by Kutateladze,<sup>1</sup> the corresponding protein can be recruited to specific intracellular compartments.

The plasma membrane is mainly composed of sterols, such as cholesterol (CHOL: neutral lipid), and lipids with PC (zwitterionic lipid), PS (anionic lipid), and PI (monovalent acidic lipid) headgroups.<sup>8,9</sup> As a minor component, the global concentration of PIPs is ~1–2% of the total phospholipids depending on the cell type.<sup>7,8,12</sup> The amount and distribution of PIPs in the cell vary significantly. While PI4P and PI(4,5)P<sub>2</sub> are constituent lipids in membranes, others are only transiently produced in response to specific stimuli or receptors.<sup>1</sup> PIPs are

Received: January 18, 2014

Revised: March 29, 2014

Published: April 1, 2014

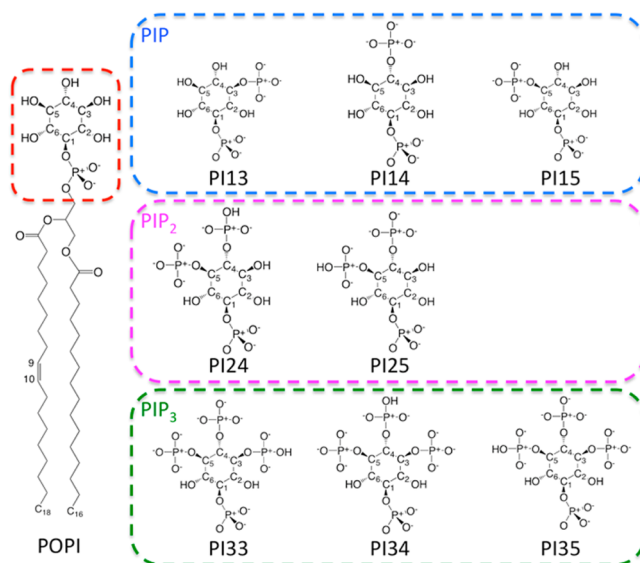


**Figure 1.** Chemical structures of POPI, PIP headgroups (PI13, PI14, and PI15), PIP<sub>2</sub> (PI24 and PI25), and PIP<sub>3</sub> (PI33, PI34, and PI35). In PIP, the different phosphorylation sites lead to PI13, PI14, and PI15, respectively. In PIP<sub>2</sub> and PIP<sub>3</sub>, the different protonation sites lead to PI24, PI25, PI33, PI34, and PI35, respectively.

highly charged lipids, e.g., at pH 7.0, PIP<sub>2</sub> is expected to have a valence of  $-4$ , because one of two phosphates is protonated.<sup>8,9</sup>

Since PIPs function as molecular beacons for distinct target proteins, in order to gain insights into the protein-PIP<sub>s</sub> recognition process, it is necessary to study the inositol ring orientation (with respect to the membrane) of PIPs with different phosphorylation sites. Since the highly abundant (20–40%)<sup>9</sup> PS lipids are known to play a key role in the recruitment of signaling proteins to the membrane surface through nonspecific electrostatic interactions,<sup>13,14</sup> it is important to understand whether PS lipids have an impact on the inositol ring orientation, as well as how proteins locate specific PIPs after being recruited to the membrane surface.

To address these questions, we have performed all-atom molecular dynamics (MD) simulations of eight heterogeneous bilayers based on yeast plasma membrane composition (CHOL/PC/PS/PI/PIP)<sup>15</sup> with 2% PIPs of various phosphorylation and protonation sites (3 PIP, 2 PIP<sub>2</sub>, and 3 PIP<sub>3</sub>; Figure 1). We also simulated the corresponding bilayers without PS to tease out the effect of PS on the behavior of PIPs, and also to explore the influence of the headgroup composition to the bilayer structure and properties. The simulation results provide a detailed picture of the interactions between headgroups of PIPs and other phospholipids. Our analysis indicates that the PS headgroup influences the inositol ring orientation of PIPs by forming substantive PS-PIP<sub>s</sub> hydrogen bonds, which also provides insights into the molecular recognition mechanism between PIPs and their target protein.

## METHODS

**Simulation Systems and Details.** A yeast-like plasma membrane model is composed of DOPC (dioleoylphosphatidylcholine), POPS (palmitoyloleoylphosphatidylserine), POPI (palmitoyloleoylphosphatidylinositol), CHOL, and PIPs.<sup>15</sup> CHOL was used as it has minimal difference in structure from ergosterol (main sterols in yeast plasma membrane).<sup>16</sup> Fatty acid chains were chosen to match the amount of chain

saturation of the yeast plasma membrane (33%).<sup>15,17</sup> In each leaflet, there are 10 DOPC, 10 POPS, 9 POPI, 1 PIP (or 1 PIP<sub>2</sub> or 1 PIP<sub>3</sub>), and 20 CHOL, leading to a 2% of PIPs concentration. Eight mixed bilayers were built of distinct PIPs with different phosphorylation and protonation sites, including 3 PIP, 2 PIP<sub>2</sub>, and 3 PIP<sub>3</sub> (see Figure 1 for the chemical structures of PI and PIPs headgroups, and PIPs naming in this study). By switching POPS to POPC, eight more mixed bilayers were constructed to investigate the impact of PS headgroup (see Table S1 for detailed system information); for brevity, the PS-containing membranes are called PS membranes and the PC-enriched membranes are called PC membranes. The snapshots of two representative yeast-like membrane models are shown in Figure 2. For simplicity, they are denoted PC\_PUPI14 (DOPC/POPC/POPI/POPI14/CHOL) and PS\_PUPI14 (DOPC/POPS/POPI/POPI14/CHOL). Table S1 contains all system names for the 16 membrane models. Assuming one of the inositol ring phosphates is protonated in PIP<sub>2</sub> and PIP<sub>3</sub> under physiological conditions,<sup>9,18</sup> the net charges on PIP, PIP<sub>2</sub>, and PIP<sub>3</sub> are  $-3e$ ,  $-4e$ , and  $-6e$ , respectively.<sup>19</sup> K<sup>+</sup> was added as a counterion to neutralize the system. The total number of atoms in each system is  $\sim 18\ 000$ , and the number of water molecules is  $\sim 2300$ .

To improve sampling and to check simulation convergence, we made three independent systems for each membrane model with different initial lipid displacement and packing, yielding a total of 48 systems. All the simulation systems were constructed using *Membrane Builder*<sup>20,21</sup> in CHARMM-GUI.<sup>22</sup> Equilibration simulations at 225 ps were performed in the standard six-step *Membrane Builder* protocol<sup>20,21</sup> for all systems using the biomolecular simulation program CHARMM<sup>23</sup> with the CHARMM36 lipid force field<sup>24</sup> and a TIP3P water model.<sup>25,26</sup> After equilibration, a 300-ns NPT (constant particle number, pressure, and temperature) production run was performed with NAMD<sup>27</sup> yielding a total of 14.4  $\mu$ s. All simulations were performed under the following protocol. A 2-fs time-step with the SHAKE algorithm<sup>28</sup> was used. The van der Waals interactions were smoothly switched off at 10–12 Å by a force-switching function,<sup>29</sup> and long-range electrostatic interactions were calculated using the particle-mesh Ewald method.<sup>30</sup> Temperature and pressure were held at 303.15 K and 1 bar, respectively. In CHARMM simulations, Langevin temperature control was used for NVT (constant particle number, volume, and temperature) dynamics. Temperature and pressure controls were achieved with a Hoover thermostat<sup>31</sup>

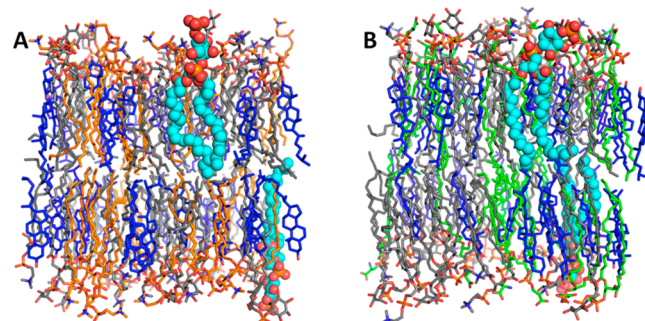


**Figure 2.** Snapshots of the yeast-like membranes at 300 ns: (A) PC\_PUPI14 (DOPC/POPC/POPI/POPI14/CHOL), (B) PS\_PUPI14 (DOPC/POPS/POPI/POPI14/CHOL), CHOL, POPC, and POPS are colored in blue, orange, and green, respectively. DOPC and POPI are colored in gray. POPI14 is shown as spheres (cyan).

and Langevin-piston<sup>32,33</sup> for NPT dynamics. For NAMD simulations, Langevin dynamics was used to maintain constant temperatures with a Langevin coupling coefficient set to 1 ps<sup>-1</sup>, and a Nosé–Hoover Langevin piston<sup>34,35</sup> was used to maintain constant pressure with a piston period set to 50 fs and piston decay of 25 fs. The simulation results are presented for the last 250 ns of each system.

#### Information Theory-Based Transfer Entropy Analysis.

To quantify the correlation and causality between PIPs–lipid interactions and inositol ring orientations of PIPs with respect to the membrane, information theory-based transfer entropy analysis<sup>36,37</sup> was performed on two time series: (1) the number of hydrogen bonds formed between inositol rings of PIPs and other phospholipid headgroups and (2) the tilt angle of PIPs inositol ring. A key step in the analysis is the symbolization, which maps the time series to finite states so that one can calculate the probability of having each state. For hydrogen bonds, the number is directly used as the symbols, whereas for tilt angles, a cutoff scheme was used. The tilt angles larger than the cutoff were classified as the “0” state, corresponding to the state when the PIPs inositol rings are close to the membrane surface; otherwise, the tilt angles were classified as “1”. Two different tilt angle cutoffs, 45° and 60°, were tested, and the results did not differ significantly. Therefore, only the results using the 45° cutoff are reported. The embedding dimension, which is the number of steps in the past to be included in the probability calculation, was set to 1, as Qi and Im previously used for protein folding analysis.<sup>36</sup> Each time series has 60 000 data points from the entire trajectories.

## RESULTS AND DISCUSSION

**Comparison of Overall Bilayer Properties between PS and PC Membranes.** The yeast-like membranes were characterized in terms of the per-lipid surface area, hydrophobic thickness, acyl chain order parameter, and density profile of heavy atoms. The surface area gives a general idea of lipid packing in the membrane surface, which can also be used to check the convergence of the simulations. To calculate the surface area of each lipid type in a heterogeneous bilayer system, we used the approach of Pandit et al.<sup>38</sup> using Voronoi tessellation. Briefly, three atoms were used to define a phospholipid, i.e., the two carbonyl carbon atoms (C21 and C31) and the middle carbon (C2) of the glycerol backbone.<sup>21</sup> Only the hydroxyl oxygen (O3) was used to define CHOL.<sup>21</sup> Figure S1 plots the time series of the average overall per-lipid surface area for 16 yeast-like mixed bilayers with 3 independent systems, showing that these systems are well equilibrated after 50 ns. The individual average surface area of each lipid type is calculated over the last 250 ns and shown in Figure S2. The average per-lipid surface area in different systems is very similar for the same lipid type. The surface area of CHOL is ~30 Å<sup>2</sup>, and the surface areas of all phospholipids are ~54–58 Å<sup>2</sup> in our simulations. Compared to the per-lipid area values in pure lipid bilayers,<sup>39,40</sup> a reduction of ~10 Å<sup>2</sup> for DOPC was observed, which is related to the addition of CHOL.

The hydrophobic thickness is one of the most important bilayer properties, which is inversely proportional to the area per lipid. The hydrophobic thickness of the bilayer was calculated by measuring the average distance between acyl chain C2 atoms (the carbon bonded to carbonyl group; see Figure 1) in the top and bottom leaflets. As shown in Figure S3, the average hydrophobic thicknesses of the corresponding PS and PC membranes are statistically identical for most systems

with the difference of less than 0.3 Å. This indicates that the hydrophobic thickness of a membrane mainly depends on the composition of the acyl chain (at least for our systems). The calculated hydrophobic thicknesses are significantly bigger than those reported in the simulation study of Kim et al.,<sup>41</sup> which are ~28–29 Å for the bulk region of the DOPC and POPC bilayers containing gramicidin A. Such a difference arises from the fact that the bilayers in our simulations are in liquid-ordered states due to a high CHOL concentration (40%).

Lipid deuterium order parameters ( $S_{CD}$ ) are a common metric for bilayer fluidity (liquid ordered versus liquid disordered). The order parameter of each C–D bond vector is defined as  $S_{CD} = \langle 3 \cos^2 \theta_{CH} - 1 \rangle / 2$  where  $\theta_{CH}$  (CH because we simulate undeuterated lipids) is the time dependent angle between the C–H bond vector and the bilayer normal (the Z-axis), and the angular bracket denotes a time and ensemble average.<sup>42</sup> The  $S_{CD}$  of the *sn*-1 chains of POPI and DOPC for the PC\_POPI14, PS\_POPI14, PC\_POPI24, and PS\_POPI24 bilayers are shown in Figure S4 (see Figure S5 for the  $S_{CD}$  of all the related lipid acyl chains). The general trends for saturated (POPI *sn*-1) and unsaturated (DOPC *sn*-1) acyl chains are in good accordance with a previous simulation study.<sup>43</sup> Local disordering is found around the double bond (C9 and C10) in unsaturated DOPC *sn*-1 chain. In addition, increasing disorder along the fatty acid chains is also observed toward the methyl groups for both chains. Due to the high CHOL concentration, the chain order is much higher than the one in a liquid-disordered state (generally well below 0.3), indicating that the membranes in this study are in a liquid-ordered state. The absolute values of  $S_{CD}$  agree well with those obtained from the previous cholesterol-containing membrane simulations.<sup>43</sup> The  $S_{CD}$  values in all systems are almost the same, indicating the uniformity of the bilayer properties of the chain region regardless of the headgroup composition in our systems.

Heavy atom density profiles along the bilayer normal (Z-axis) for water and lipid components (carbon tail, headgroups, carbonyl group, CHOL ring, and CHOL tail) are shown in Figure S6 and compared for the corresponding PS and PC membranes. As expected from the hydrophobic thickness and  $S_{CD}$  comparisons, there is no impact of the PS headgroup on the density profiles of the acyl chain, and the same conclusion can also be applied to the spatial distributions of headgroup atoms. The headgroup–headgroup thickness is identical for PC\_POPI4 and PS\_POPI14 (Figure S6A), as well as all the other systems. Therefore, structural properties of the corresponding PS and PC membranes in this study are uniform.

The orientation of CHOL was also obtained by measuring the tilt angle of the cholesterol ring, which is defined by the vector connecting C3 and C17 with respect to the bilayer normal.<sup>44</sup> Figure S7 shows no apparent difference in the distributions of CHOL ring orientation in the corresponding PS and PC membranes, which further verifies the similarity of their bilayer structures. The mean values (~14–15°) of the tilt angles are also consistent with the <sup>2</sup>H NMR experimental study (15–16°)<sup>45</sup> for CHOL in PE and PC membranes with saturated and/or monounsaturated acyl chains and other simulation studies (~12–19°) with ~10–20% of CHOL.<sup>21</sup>

**PIP<sub>n</sub> Inositol Ring Position and Orientation.** In order to better understand the protein-PIP<sub>n</sub> recognition mechanisms, it is essential to examine the position and orientation of PIP<sub>n</sub> inositol ring headgroup in a bilayer. The average Z-positions of the headgroup phosphates of DOPC, POPI, POPC/POPS, and phosphates on the PIP<sub>n</sub> inositol rings are presented in Table S2

and Figure 3; the bilayer center is located at  $Z = 0$ . Compared to the phosphate positions of PC, PS, and PI headgroups ( $\sim 22\text{--}23 \text{ \AA}$ ), it is evident that phosphate groups on the PIP inositol rings ( $\sim 27\text{--}30 \text{ \AA}$ ) mostly stay above the membrane surface or other lipid headgroups, which is also observed in other simulation studies.<sup>12,19</sup> Even though the main phosphate (directly connected to glycerol backbone) positions do not show differences between PC and PS membranes (Table S2), it is interesting to note that at least one of the phosphate groups on the PIPs inositol rings in PC membranes are  $\sim 1 \text{ \AA}$  farther from the bilayer center than those in PS membranes (Figure 3). This is somewhat unexpected, because, considering only the anionic character of PIPs and PS lipids, this would result in an energetically unfavorable interaction. In fact, the zwitterionic PC headgroups have a positively charged choline that could electrostatically attract the negative phosphates of PIPs. In addition, if the solvation energy of the PIPs inositol ring is the main determinant of its position and orientation, there should be no difference between the PS and PC membranes, i.e., the inositol ring would stay away from the membrane surface regardless of PS or PC membranes. This puzzling observation is further elucidated in detail after the orientation of the PIPs inositol ring is described.

The orientation of the inositol ring is characterized by its tilt angle ( $\theta$ ) and rotation angle ( $\varphi$ ). As shown in Figure 4, the tilt angle is defined by the C1–C4 vector ( $v_{14}$ ) with respect to the bilayer normal ( $Z$ ), which was also used by Li et al. in their simulation study.<sup>19</sup> The rotation angle was defined as the angle between the projection of the C3–C5 vector ( $v_{35}$ ) and the projection of the Z-axis ( $z_p$ ) on the plane perpendicular to  $v_{14}$ . In this way,  $\varphi$  does not depend on  $\theta$ ; see below for the detailed explanation. The tilt angle distributions of PIPs and POPI inositol rings are compared in Figure 5 for PC\_POPI14, PC\_POPI24, PS\_POPI14, and PS\_POPI24 (see Figure S8 for the  $\theta$  distribution of the other systems). The general behaviors of these 4 representative systems are similar. The distribution of POPI inositol rings is very broad, which covers a wide range ( $0\text{--}160^\circ$ ), indicating POPI inositol rings are very flexible. These inositol rings can swing back and forth on the membrane surface, sometimes with the ring pointing down ( $\theta > 90^\circ$ ). However, the PIPs inositol rings mostly point up (more than 95% of time except PS\_POPI15 with 84%) with smaller tilt angles ( $\theta < 90^\circ$ ) and are less flexible with an average value of 34–59°. This is likely due to the solvation energy of the inositol ring phosphate group that forces the ring to stay away from the

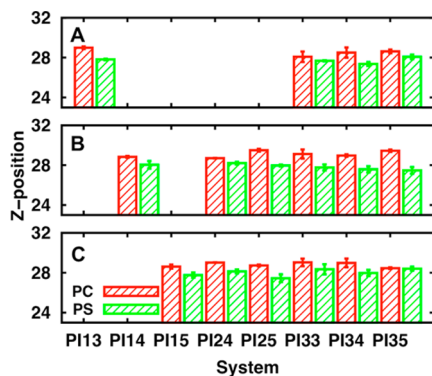


**Figure 3.** Average Z-positions of the phosphates P3 (A), P4 (B), and P5 (C) in PIP, PIP<sub>2</sub>, and PIP<sub>3</sub> in the PC (red) and PS (green) membranes.

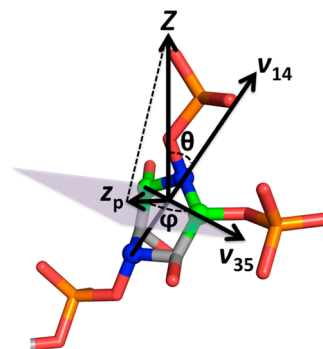


**Figure 4.** Definitions of the inositol ring tilt angle ( $\theta$ ) and rotation angle ( $\varphi$ ). The tilt angle ( $\theta$ ) is defined as the angle between the vector ( $v_{14}$ ) connecting C1 and C4 atoms (blue spheres) and the bilayer normal ( $Z$ ). The rotation angle ( $\varphi$ ) is defined as the angle between the projection of the vector ( $v_{35}$ ) connecting C3 and C5 atoms (green spheres) and the projection of the  $Z$ -axis ( $z_p$ ) on the plane (light purple) perpendicular to  $v_{14}$ . The molecule shown is a PI24 headgroup taken from a representative snapshot of the MD simulations, and hydrogen atoms are not shown for clarity.

membrane surface (see below). The average tilt angle obtained for PIP<sub>2</sub> and PIP<sub>3</sub> in a POPC bilayer in Li et al.'s 50-ns simulations is  $50^\circ$  (i.e.,  $40^\circ$  with respect to the bilayer surface),<sup>19</sup> which also falls into the range observed in our simulations. Figure 6 compares the tilt angle distributions between the corresponding PS and PC membranes for all PIPs. It is obvious that, compared to PC\_POPI15 and PC\_POPI34, the inositol ring tilt angle distributions in PS\_POPI15 and PS\_POPI34 membranes shift to the right (i.e., larger tilt angles), leading to a second peak with larger tilt angles ( $\sim 80\text{--}100^\circ$ ). The same feature does exist in other systems while it is less obvious than in PC\_POPI15 and PC\_POPI34. This suggests that there is an increase in the ring population to tilt more toward the membrane surface in PS membranes compared to PC membranes, which is also consistent with the inositol ring phosphate groups being closer to the membrane surface in PS membranes (Figure 3). Interestingly, there was no impact of the increased tilt angle on the position of the PIPs acyl chains along the  $Z$ -axis in PS\_POPI15 and PS\_POPI34 (data not shown).

Two-dimensional populations of PIPs tilt angles and their glycerol torsions<sup>24</sup>  $\beta_1$ ,  $\theta_2$ , and  $\theta_4$  were calculated and compared among all the different PIPs bilayers (Figure S9). The overall patterns of the distribution of three torsion angles are very similar between different systems with equally populated  $75^\circ$  and  $150^\circ$  for  $\beta_1$ , and mostly  $60^\circ$  and  $300^\circ$  with small populations of  $180^\circ$  for  $\theta_2$  and  $\theta_4$ . When tilt angles increase in PS\_POPI15 and PS\_POPI34,  $\beta_1$  slightly prefers  $75^\circ$  over  $150^\circ$  and  $\theta_4$  mainly prefers the torsion angle of  $75^\circ$ , while no obvious preference of  $\theta_2$  was found. Compared to the glycerol torsion surfaces of 1,2-dipalmitoyl-sn-phosphatidylcholine (DPPC) reported by Klauda et al.,<sup>24</sup> our study shows a good agreement for  $\beta_1$  and a reduction of  $180^\circ$  for  $\theta_2$  and  $\theta_4$  of PIPs.

Figure 7A illustrates the relative inositol ring orientations with respect to the membrane surface based on  $\varphi$  defined in Figure 4. The C3–C5 vector stays parallel to the membrane surface when  $\varphi = 90^\circ$  or  $270^\circ$ . For  $0^\circ \leq \varphi < 90^\circ$  or  $270^\circ < \varphi \leq 360^\circ$ , the C3 side of the ring faces down and is closer to the membrane surface, and vice versa for  $90^\circ < \varphi < 270^\circ$  (i.e., the C5 side of the ring faces down at  $\varphi = 180^\circ$ ). The  $\varphi$

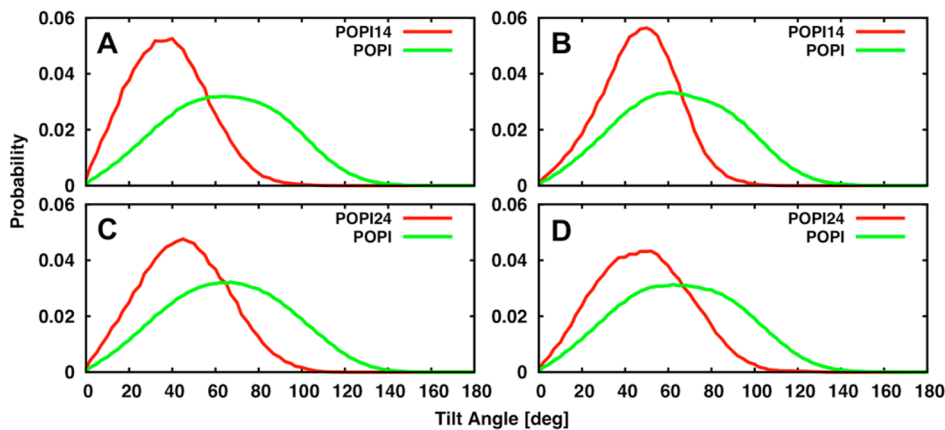


**Figure 5.** Tilt angle distributions of PIP/PIP<sub>2</sub> (red) and POPI (green) headgroups for (A) PC\_POPI14, (B) PS\_POPI14, (C) PC\_POPI24, and (D) PS\_POPI24.

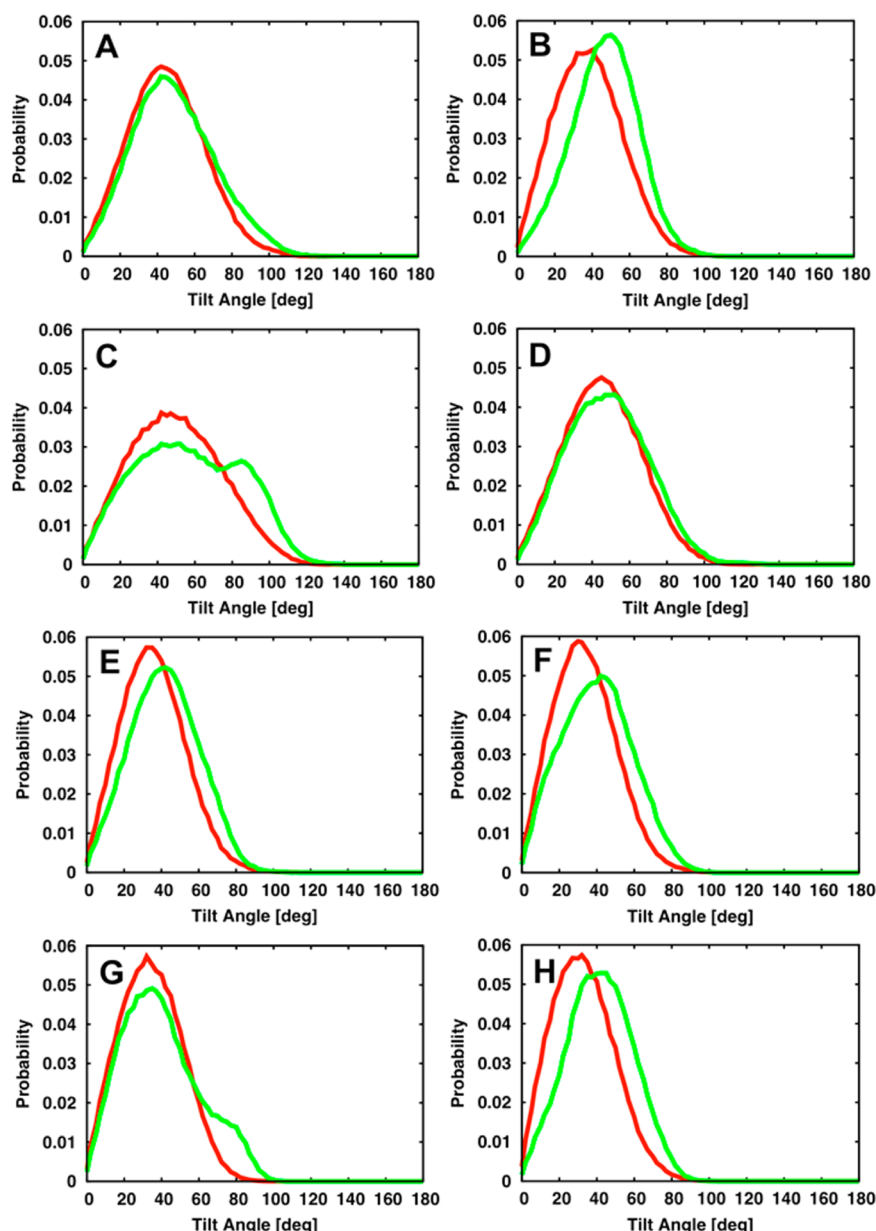


**Figure 6.** PIP, PIP<sub>2</sub>, and PIP<sub>3</sub> inositol ring tilt angle distribution comparison between the PC (red) and PS (green) membranes for (A) POPI13, (B) POPI14, (C) POPI15, (D) POPI24, (E) POPI25, (F) POPI33, (G) POPI34, and (H) POPI35.

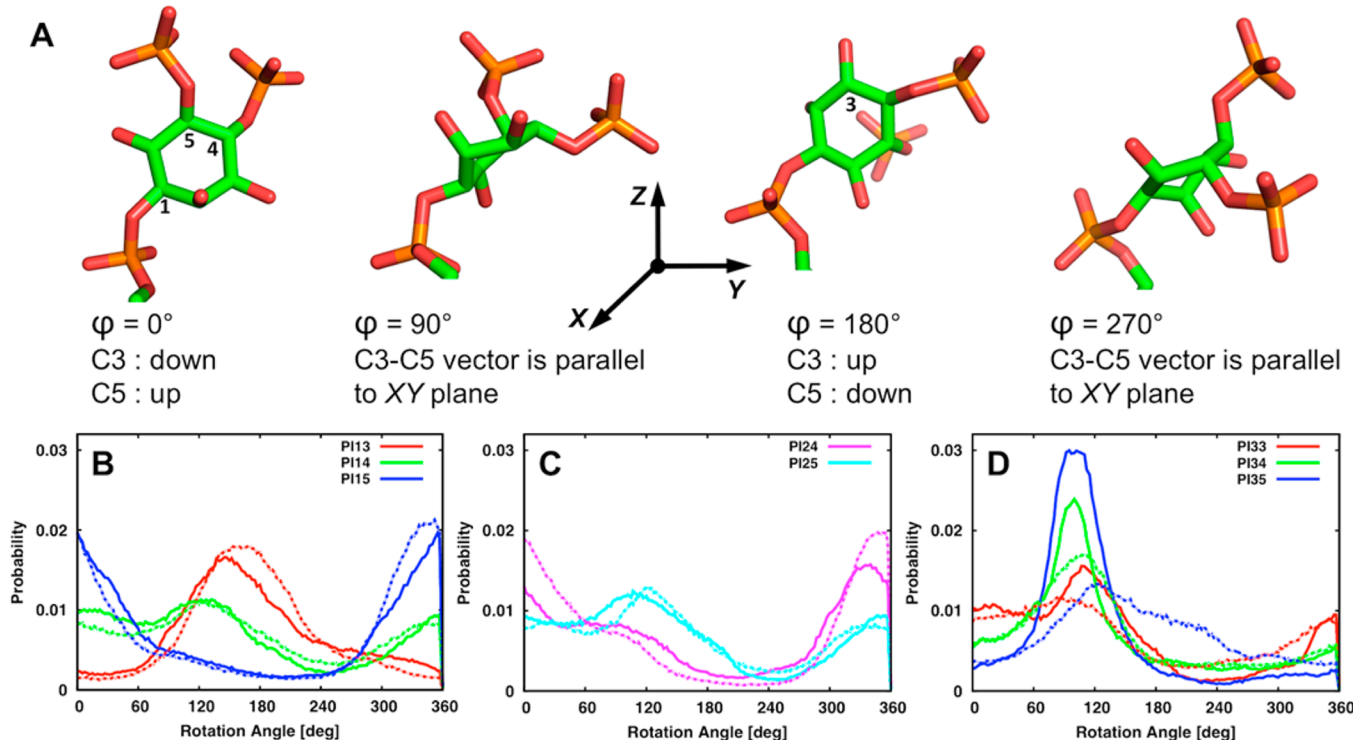


**Figure 7.** (A) Representative snapshots with PI24 inositol ring rotation angle  $\varphi$  of  $0^\circ, 90^\circ, 180^\circ$ , and  $270^\circ$  with a tilt angle of  $45^\circ$ . Atom numbers of the carbons in the inositol ring are also shown for C1, C3, C4, and C5. The rotation angle distributions of (B) PIP, (C)  $\text{PIP}_2$ , and (D)  $\text{PIP}_3$ . The solid lines are for the PS membranes and the dashed lines are for the PC membranes.

distributions of the inositol ring in both the PS and PC membranes are shown in Figure 7B–D. Overall, switching headgroups between PC and PS makes little difference on the  $\varphi$  distribution patterns. However, a clear difference is observed between different PIPs. For PIP (Figure 7B), PI13 favors the orientation with  $\varphi$  ( $\sim 150^\circ$ ) in between  $90^\circ$  and  $270^\circ$ , so the C3 atom of the ring, to which the phosphate group is attached, stays farther away from the membrane surface. In this way, it maximizes the favorable solvation energy of the phosphate group on C3. Since PI14 has a relatively symmetric structure without considering its stereoisomerism (Figure 1), its distribution is much broader with no preference for either C3 or C5 side of the ring being closer to the membrane surface. In the case of  $\text{PIP}_2$  (Figure 7C), PI24 has a similar distribution to PI15 because they have the same unprotonated phosphate group on the C5 position (Figure 1). The PI24 and PI25 headgroups are very similar in terms of the position of the inositol ring phosphate groups, so the distribution difference mainly comes from the charge difference between C4 and C5 positions (i.e., protonation sites). Compared to PI24, PI25 has less charge on the C5 side of the ring, which leads to the distribution slightly in favor of the rotation angles with the C5 side of the ring toward the membrane surface. Since lowering the charge density of the phosphate group on the C5 side also makes the  $\text{PIP}_2$  molecule more symmetric in terms of charge distribution, the distributions of PI25 and PI14 are very similar. For  $\text{PIP}_3$  (Figure 7D), to maximize favorable solvation energy with three phosphate groups (see below), the inositol ring C3–C5 vector mostly stays flat ( $\varphi = \sim 90^\circ$ ), meaning that C3 and C5 atoms are at similar height due to the molecular symmetry. Protonation slightly influences the orientation, resulting in minor difference between PI33, PI34, and PI35. Li et al. reported a multiple-minima rotation angle distribution for  $\text{PIP}_2$

and  $\text{PIP}_3$  in a POPC bilayer, with the inositol ring staying flat or either P3 or PS being higher than the other.<sup>19</sup> As shown in Figure 7, there are no obvious multimodal distributions in our cases. This discrepancy could arise from the insufficient sampling in their relatively short simulations.

Figure 8 is the two-dimensional distribution of the solvent-accessible surface area (SASA) of PIPs headgroups as a function of PIPs inositol ring tilt and rotation angle for replica 2 of PS\_POPI15 and PS\_POPI34, where a second peak with larger

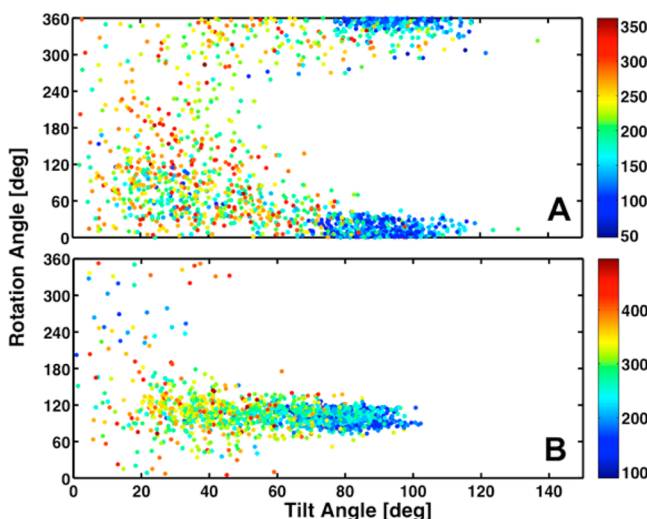


**Figure 8.** Two-dimensional PIPs headgroup solvent-accessible surface area (SASA) distributions as a function of PIPs inositol ring tilt and rotation angles for (A) PS\_POPI15 replica 2 and (B) PS\_POPI34 replica 2.

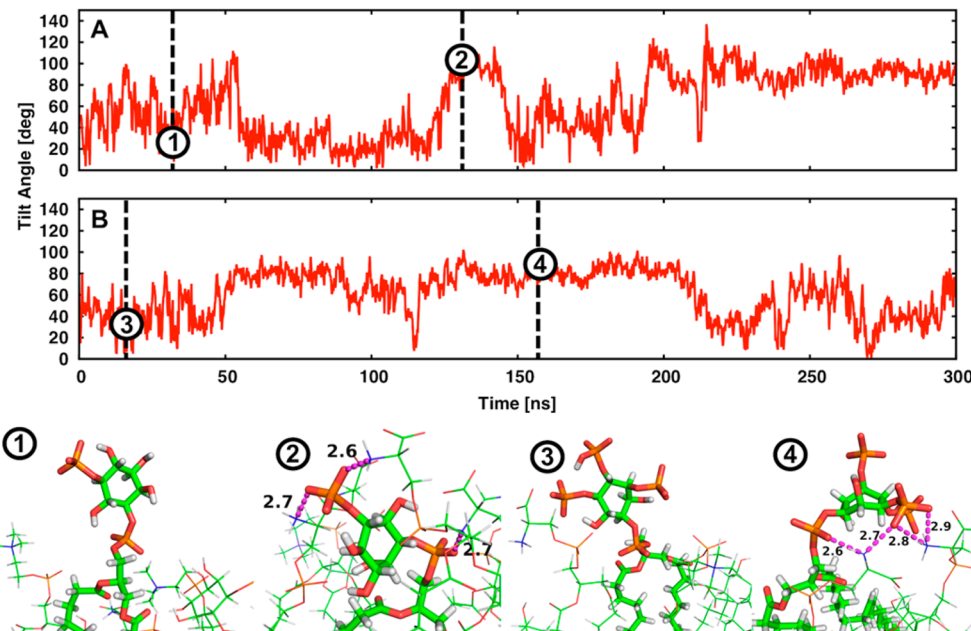


**Figure 9.** Time-series of the inositol ring tilt angles for (A) PS\_POPI15 replica 2 and (B) PS\_POPI34 replica 2. The snapshots show the residues within 4 Å of POPI15 headgroup [at ① 30 ns and ② 128 ns] and POPI34 headgroup [at ③ 21 ns, and ④ 157 ns]. PIP/PIP<sub>3</sub> are shown in stick representation and others in line representation. The magenta dashed lines represent hydrogen bonds formed between PIP/PIP<sub>3</sub> and PS headgroups. The corresponding distance between donor and acceptor is shown in black.

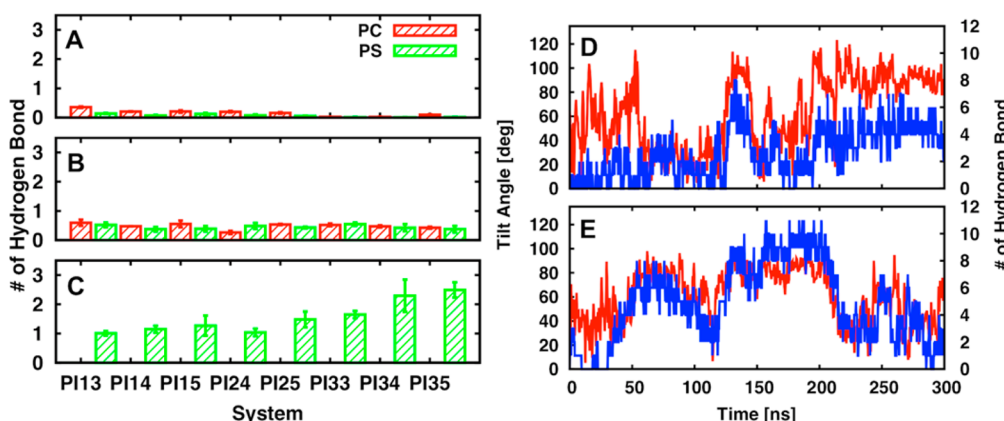


**Figure 10.** Average numbers of hydrogen bonds formed between the inositol ring of PIP, PIP<sub>2</sub>, and PIP<sub>3</sub> and (A) PC headgroup in the PC (red) and PS (green) membranes; (B) PI headgroup in the PC (red) and PS (green) membranes; and (C) PS headgroup with standard errors over three replicas. Time-series of the inositol ring tilt angle (red) and the hydrogen bond numbers (blue) for (D) PS\_POPI15 replica 2 and (E) PS\_POPI34 replica 2.

tilt angles of 80–100° was observed (Figure 6C and G). Clearly, the accessible rotation angles become restricted as the tilt angles increase, which is similar to the tilt-rotation relationships found in transmembrane  $\alpha$ -helices and  $\beta$ -sheets.<sup>41,46–49</sup> In addition, the SASA value generally decreases as the tilt angle increases to a certain degree, indicating that the favorable solvation energy reduces when the PIPs headgroup is closer to the membrane surface. It also illustrates that the solvation energy is the driving force of the decreased flexibility of the PIPs headgroup tilt angle distribution compared to that of the PI headgroup in Figure 5. However, it raises a question about what compensates for the loss of the favorable solvation energy when the tilt angle is larger in these two systems.

**Impact of Lipid Headgroup Interactions on Inositol Ring Orientation.** To better understand the reason the inositol rings have an unexpected tendency of staying closer to

the membrane surface in the PS membranes compared to the PC membranes (Figures 3 and 6), the interactions between the inositol ring of PIPs and other lipid headgroups are further characterized. Again, the PS\_POPI15 and PS\_POPI34 systems are used as the representative systems to monitor the time series of inositol ring tilt angle (Figure 9A,B). Figure 9 also shows four snapshots of residues within 4 Å of each inositol ring at 30 ns (①) and 128 ns (②) in PS\_POPI15 and at 21 ns (③) and 157 ns (④) in PS\_POPI34 from the top leaflet. In snapshots ② and ④ with larger tilt angles (98° and 83°), various hydrogen bonds are observed between PS headgroups and inositol ring phosphate groups. On the other hand, in snapshots ① and ③ with smaller tilt angles of 18° and 23°, there was no hydrogen bond formed. This suggests that hydrogen bond formation between headgroups is pivotal for stabilizing the

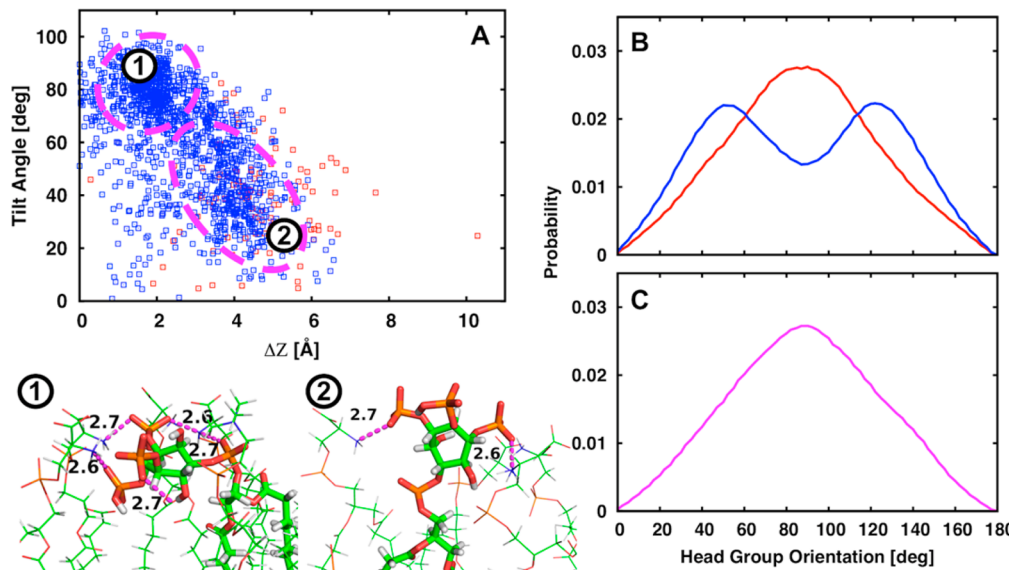


**Figure 11.** (A) Inositol ring tilt angle as a function of the Z-distance ( $\Delta Z$ ) from the headgroups of PS/PI/PC (within 7 Å of  $\text{PIP}_3$  headgroup) to the  $\text{PIP}_3$  headgroup for PS\_POPI34 replica 2: red for the  $\text{PIP}_3$  headgroup without hydrogen bonds formed and blue for the  $\text{PIP}_3$  headgroup with hydrogen bonds formed. Two representative snapshots (bottom) are chosen from ① 136.2 ns and ② 114.4 ns.  $\text{PIP}_3$  is shown in stick representation and others in line representation. The magenta dashed lines represent hydrogen bonds formed between  $\text{PIP}_3$  and PS/PI headgroups. The corresponding distance between donor and acceptor is shown in black. (B and C) Tilt angle distributions in PS\_POPI34 for PS headgroup and PI headgroup. Headgroup tilt angles are defined by  $\text{P}-\text{NH}_3^+$  (red) and  $\text{P}-\text{COO}^-$  (blue) vectors for PS, and  $\text{P}-\text{C4}$  (magenta) vector for PI with respect to the bilayer normal ( $Z$ ).

conformation with larger tilt angles and might be responsible for the tilt angle distribution shift in the PS membranes.

Figure 10A–B shows that there is no significant difference in the number of hydrogen bonds formed between the inositol ring of PIPs and the headgroups of PC/PI in the PC and PS membranes. However, since PS headgroup is a better hydrogen bond donor compared to PC, much more hydrogen bonds are formed in the PS membranes for all the different PIPs bilayers (Figure 10C). This is consistent with the increased population (up to 20% for POPI14 and POPI35) of their inositol ring closer to the membrane surface in the PS membranes. In general,  $\text{PIP}_3$  is capable of forming more hydrogen bonds with adjacent lipids compared to PIP and  $\text{PIP}_2$  due to more phosphate groups, although the local arrangement of different lipids also matters. In the recent experimental study with  $\text{PIP}_2$ /PS/PC lipid vesicles, Gruber et al. found that the effect of PS on  $\text{PIP}_2$  ionization is minor, which was unexpected since the presence of PS headgroups will increase the negative interfacial charge and could result in a reduced interfacial pH.<sup>7</sup> Their findings suggest that either  $\text{PIP}_2$  demixes from PS or that the effect is countered by the hydrogen bond formation between PS ammonium groups and PIPs inositol ring phosphomonoester groups. Our simulations support the latter explanation. This universal behavior of hydrogen bond formation in all PS membranes might be potentially important for the protein-PIP<sub>n</sub> recognition events.

To further verify the effect of hydrogen bonding on the inositol ring tilt angle distribution, the time-series of the number of hydrogen bonds (blue) between PIPs inositol ring and PC/PI/PS headgroups is compared with the tilt angle (red) time-series for PS\_POPI15 (Figure 10D) and PS\_POPI34 (Figure 10E). In general, the number of hydrogen bonds correlates very well with the behavior of tilt angle. When the tilt angle decreases, the number of hydrogen bonds decreases as well. The Pearson correlation coefficient is 0.57 for PS\_POPI15

and 0.68 for PS\_POPI34; the corresponding *P*-value is less than  $10^{-3}$ , indicating some correlations between the two time series. In such cases, do the hydrogen bonds drive the inositol ring tilting or vice versa? Information theory-based transfer entropy (TE) analysis<sup>36,37</sup> was employed to explore the causality relationship between the number of hydrogen bonds (HB) and PIPs tilt angle ( $\theta$ ). The outcome of the TE analysis is a normalized directional index  $D_{\text{HB} \rightarrow \theta}$  which is positive if there is information flow from HB to  $\theta$ , and vice versa. The  $D_{\text{HB} \rightarrow \theta}$  of PS\_POPI34 is 0.1, indicating that the formation of hydrogen bonds drives the change of the tilt angle.  $D_{\text{HB} \rightarrow \theta}$  of PS\_POPI15 is smaller (0.06). While the calculated  $D_{\text{HB} \rightarrow \theta}$  values are small due to limited simulation time scale for these system (c.f., hundreds of microsecond simulations were used in the previous protein folding analysis),<sup>36</sup> these values are still significantly indicative of the causality between HB and  $\theta$ .

Although hydrogen bonds and tilt angles are well correlated in one of the replicas of PS\_POPI15 and PS\_POPI34, inconsistent behaviors with small tilt angle and various hydrogen bonds formed are not rare in other replicas as well as other systems. Therefore, while the hydrogen bond formation is an important determinant, it is not the sole contributor to the inositol ring tilt angle distribution shift in Figure 6. As shown in Figure 11A, the PIPs inositol ring orientations without hydrogen bond formation with lipid headgroups (red) tend to have smaller tilt angles, while the conformations with hydrogen bonds (blue) sampled from PS\_POPI34 can be roughly divided into two regions. Two representative snapshots are also shown in Figure 11. Snapshot ① has a larger tilt angle ( $87^\circ$ ) and a smaller distance ( $0.01$  Å) along Z-axis between  $\text{PIP}_3$  headgroup and its surrounding lipid headgroups, while snapshot ② has a smaller tilt angle ( $25^\circ$ ) and a larger distance ( $3.3$  Å) between headgroups. Considering that the average distance between PIPs inositol ring and other lipid headgroups along the Z-axis is  $\sim 6$  Å (Table S2), Figure 11A

clearly shows a smaller  $\Delta Z$  in region 2, indicating that surrounding lipid headgroups can be elevated and proximate to PIPs inositol ring to form hydrogen bonds even in small tilt angles.

The orientation of the PS and PI headgroups, which are PIPs' hydrogen bond partners, has a determinant effect on the calculated  $\Delta Z$  and observed tilt angles of PIPs inositol ring. Figure 11B shows the headgroup tilt angle distributions of P-NH<sub>3</sub><sup>+</sup> (red) and P-COO<sup>-</sup> (blue) vectors for PS lipids, and Figure 11C displays that of the P-C4 vector for PI lipids. For PS lipids, the P-NH<sub>3</sub><sup>+</sup> group is approximately parallel ( $\sim 90^\circ$ ) to the membrane surface with the COO<sup>-</sup> group either protruding from the membrane surface ( $<90^\circ$ ) or submerged under the membrane surface ( $>90^\circ$ ). For PI, the P-C4 vector tends to be predominantly parallel to the membrane surface ( $\sim 90^\circ$ ). The general preference of the phospholipid headgroups to be parallel to the membrane plane was also mentioned in McLaughlin's review.<sup>9</sup> However, as shown in Figure 11B–C, the distributions are very broad. When the tilt angles of P-NH<sub>3</sub><sup>+</sup> (for PS lipids) and P-C4 (for PI lipids) are close to 90°, the headgroups would be parallel to the membrane and encourage a hydrogen bond (or salt-bridge) orientation with a small  $\Delta Z$  that produces a large tilt angle of PIP (Figure 11 ①). In contrast, when P-NH<sub>3</sub><sup>+</sup>/P-C4 are oriented at  $<90^\circ$ , PS/PI headgroups will be protruding from the membrane and PIPs will interact with them and form hydrogen bonds with smaller tilt angles and larger  $\Delta Z$  (Figure 11 ②). The large  $\Delta Z$  is due to the hydrogen bond interactions occurring below the tip of PIPs inositol ring. These interaction patterns also explain that although PIPs form more hydrogen bonds in all the PS membranes compared to their corresponding PC membranes (Figure 10A–C), POPI13 and POPI24 show no significant shift to larger tilt angles in Figure 6A and D. In addition, even in PC membranes, PIPs can still form hydrogen bonds with PI (Figure 10B), which impacts the inositol ring tilt angle in the same way as PS in the PS membrane.

## CONCLUSIONS

PIP are minor phospholipids in terms of quantity, yet they are vital to major signal transduction pathways by functioning as docking sites for signaling effectors.<sup>1,6</sup> In this work, we present an MD simulation study of eight yeast-like plasma membranes (DOPC/POPS/POPI/CHOL) with 2% PIPs of different phosphorylation and protonation sites to explore the PIPs inositol ring orientation. In addition, MD simulations of the corresponding bilayers with PS headgroup switched to PC were also performed to characterize the effect of the PS headgroup on inositol ring orientation, and also on membrane structure and properties. Our study shows that the bilayer properties are very similar between the PS and PC membranes in terms of per-lipid area, hydrophobic thickness, heavy atom density profile, and acyl chain order parameters, indicating that the bilayer properties are dominated by acyl chain composition instead of lipid headgroups when in a liquid-ordered state like our systems (40% cholesterol concentration).

Our study further elucidates that the solvation energy is the main driving force to determine the PIPs inositol ring orientation, especially in the case of its rotation angle. It is very clear that each PIP lipid type has its own favored orientation due to different phosphorylation and protonation sites. For the inositol ring tilt angle, it is a complicated story that involves a combination of different interactions and factors. In addition to the solvation energy, hydrogen bond formation

between lipid headgroups (PS and PI) and the PIPs inositol ring also exhibits significant impact on its distribution. Hydrogen bonds can effectively dissipate the negative charge,<sup>7</sup> reduce the electrostatic repulsion, and stabilize the inositol ring orientation with a larger tilt angle and closer to the membrane surface. As PS is a better hydrogen bond donor compared to PC, more hydrogen bonds are observed in the PS membranes. The ramification of this increased hydrogen bonding is a tilt angle distribution shift in various degrees in all the PS membrane systems, and significant distribution shifts are observed in PS\_POPI15 and PS\_POPI34 due to stable hydrogen bond formation in one of their replicas. One more factor contributing to the PIPs inositol ring tilt is the PS and PI headgroup orientation. The tilt angle distribution is only influenced by hydrogen bond formation when the relative Z-heights of PIPs inositol ring and its partner are different.

Corbin et al. have suggested a two-step search mechanism based on the study on GRP1 PH domain and PIP<sub>3</sub>.<sup>50</sup> First, the PH domain forms transient and weak electrostatic interactions with the background anionic lipids (PS/PI), which facilitates a two-dimensional search for PIP<sub>3</sub> by increasing the residency time of the protein on the membrane surface. Then, once PIP<sub>3</sub> is found, the PH-domain binds specifically to PIP<sub>3</sub> with high affinity.<sup>13,50</sup> In their model, PIP<sub>3</sub> is isolated from PS/PI, which is different from our finding that the inositol ring of PIPs can form a hydrogen bond network with PS and PI headgroups. This hydrogen bond network might be biologically important and crucial in filling the gap in the protein-PIP<sub>3</sub> recognition mechanism. Here, combined with Corbin et al.'s model and our simulations,<sup>13,50</sup> we propose a three-step protein-PIP<sub>3</sub> recognition mechanism as follows. First, proteins are attracted to the membrane surface by the anionic lipids (PS and PI) through nonspecific electrostatic interaction, which reduces the search space from three dimensions to two dimensions. This weak interaction is also perfect for efficient protein diffusion without tight binding. Second, one possible scenario is that during 2D diffusion, proteins encounter their target PIPs in a different region, which are bound to adjacent anionic lipids (PS and PI) via hydrogen bonding. Another possible scenario is that proteins can locate target PIP<sub>3</sub> by orientational changes, when PIPs are bonded to the PS/PI in the same region. Last, proteins bind to PIPs through specific interaction with inositol ring phosphate groups or a stronger nonspecific electrostatic interaction to basic residues in the protein. The information gained from this study should be beneficial in future studies exploring the details of the protein-PIP<sub>3</sub> interactions and recognition in biological environments, which is important for potential therapeutic applications of the disorders caused by misreading of PIP-involved signaling.<sup>51–55</sup>

## ASSOCIATED CONTENT

### S Supporting Information

System information (Table S1). Average Z-positions of the headgroup phosphates of DOPC, POPI, POPC/POPS, and phosphates in PIP, PIP<sub>2</sub>, and PIP<sub>3</sub> inositol rings (Table S2). Time-series of the average per-lipid surface areas of three independent systems (Figure S1). Average per-lipid surface area of each lipid type in the PC and PS membranes (Figure S2). Average hydrophobic thickness with standard errors over three replicas in the PC and PS membranes (Figure S3). Deuterium order parameters for POPI and DOPC *sn*-1 chains of PC\_POPI14, PS\_POPI14, PC\_POPI24, and PS\_POPI24 (Figure S4). Deuterium order parameters for POPI *sn*-1 and

*sn*-2, DOPC *sn*-1 and *sn*-2, and POPC/POPS *sn*-1 and *sn*-2 chains in each bilayer system (Figure S5). Density profiles of water molecule, lipid headgroup, lipid carbon tail, lipid carbonyl group, cholesterol ring, and cholesterol tail along the bilayer normal for each bilayer system (Figure S6). Probability distribution of cholesterol ring tilt angle with respect to the bilayer normal for each bilayer system (Figure S7). Inositol ring tilt angle distributions of PIP/PIP<sub>2</sub>/PIP<sub>3</sub> and POPI headgroups in each bilayer system (Figure S8). Two-dimensional populations of PIPs inositol ring tilt angle and glycerol backbone dihedral angles (Figure S9). This material is available free of charge via the Internet at <http://pubs.acs.org>.

## AUTHOR INFORMATION

### Corresponding Author

\*Phone: (785) 864-1993; Fax: (785) 864-5558; E-mail: wonpil@ku.edu.

### Present Address

Wonpil Im, Department of Molecular Biosciences and Center for Bioinformatics, The University of Kansas, Lawrence, Kansas 66047, United States

### Notes

The authors declare no competing financial interest.

## ACKNOWLEDGMENTS

We are grateful to Richard Pastor and Richard Venable for providing us with the parameters of PIPs prior to their publication. This work was supported in part by NSF MCB-1157677, NSF ABI-1145987, HFSP RGP0064/2011, and TeraGrid/XSEDE resources (TG-MCB070009).

## REFERENCES

- (1) Kutateladze, T. G. Translation of the Phosphoinositide Code by PI Effectors. *Nat. Chem. Biol.* **2010**, *6* (7), S07–S13.
- (2) Heilmann, I. Using Genetic Tools to Understand Plant Phosphoinositide Signalling. *Trends Plant Sci.* **2009**, *14* (3), 171–179.
- (3) Fairn, G. D.; Grinstein, S. Precursor or Charge Supplier? *Science* **2012**, *337* (6095), 653–654.
- (4) Di Paolo, G.; De Camilli, P. Phosphoinositides in Cell Regulation and Membrane Dynamics. *Nature* **2006**, *443* (7112), 651–657.
- (5) D'angelo, G.; Vicinanza, M.; Di Campli, A.; De Matteis, M. A. The Multiple Roles of PtdIns(4)P - Not Just the Precursor of PtdIns(4,5)P<sub>2</sub>. *J. Cell Sci.* **2008**, *121* (12), 1955–1963.
- (6) Hammond, G. R. V.; Fischer, M. J.; Anderson, K. E.; Holdich, J.; Koteci, A.; Balla, T.; Irvine, R. F. PI4P and PI(4,5)P<sub>2</sub> Are Essential But Independent Lipid Determinants of Membrane Identity. *Science* **2012**, *337* (6095), 727–730.
- (7) Gruber, Z. T.; Jiang, Z. P.; Gericke, A.; Kooijman, E. E. Phosphatidylinositol-4,5-Bisphosphate Ionization and Domain Formation in the Presence of Lipids with Hydrogen Bond Donor Capabilities. *Chem. Phys. Lipids* **2012**, *165* (6), 696–704.
- (8) McLaughlin, S.; Murray, D. Plasma Membrane Phosphoinositide Organization by Protein Electrostatics. *Nature* **2005**, *438* (7068), 605–11.
- (9) McLaughlin, S.; Wang, J.; Gambhir, A.; Murray, D. PIP(2) and Proteins: Interactions, Organization, and Information Flow. *Annu. Rev. Biophys. Biomol. Struct.* **2002**, *31*, 151–75.
- (10) Golebiewska, U.; Kay, J. G.; Masters, T.; Grinstein, S.; Im, W.; Pastor, R. W.; Scarlata, S.; McLaughlin, S. Evidence for a Fence That Impedes the Diffusion of Phosphatidylinositol 4,5-Bisphosphate out of the Forming Phagosomes of Macrophages. *Mol. Biol. Cell* **2011**, *22* (18), 3498–3507.
- (11) Lemmon, M. A. Phosphoinositide Recognition Domains. *Traffic* **2003**, *4* (4), 201–13.
- (12) Luyyan, D.; Mezei, M.; Logothetis, D. E.; Osman, R. A Molecular Dynamics Investigation of Lipid Bilayer Perturbation by PIP2. *Biophys. J.* **2010**, *98* (2), 240–7.
- (13) Lumb, C. N.; Sansom, M. S. P. Finding a Needle in a Haystack: The Role of Electrostatics in Target Lipid Recognition by PH Domains. *Plos. Comput. Biol.* **2012**, *8* (7), e1002617.
- (14) Yeung, T.; Gilbert, G. E.; Shi, J.; Silvius, J.; Kaps, A.; Grinstein, S. Membrane Phosphatidylserine Regulates Surface Charge and Protein Localization. *Science* **2008**, *319* (5860), 210–3.
- (15) van Meer, G.; Voelker, D. R.; Feigenson, G. W. Membrane Lipids: Where They Are and How They Behave. *Nat. Rev. Mol. Cell. Biol.* **2008**, *9* (2), 112–124.
- (16) Czub, J.; Baginski, M. Comparative Molecular Dynamics Study of Lipid Membranes Containing Cholesterol and Ergosterol. *Biophys. J.* **2006**, *90* (7), 2368–2382.
- (17) Daum, G.; Tuller, G.; Nemec, T.; Hrastnik, C.; Balliano, G.; Cattel, L.; Milla, P.; Rocco, F.; Conzelmann, A.; Vionnet, C.; et al. Systematic Analysis of Yeast Strains with Possible Defects in Lipid Metabolism. *Yeast* **1999**, *15* (7), 601–614.
- (18) Vanparidon, P. A.; Dekrijff, B.; Ouwerkerk, R.; Wirtz, K. W. A. Polyphosphoinositides Undergo Charge Neutralization in the Physiological pH Range - a P-31-NMR Study. *Biochim. Biophys. Acta* **1986**, *877* (1), 216–219.
- (19) Li, Z.; Venable, R. M.; Rogers, L. A.; Murray, D.; Pastor, R. W. Molecular Dynamics Simulations of PIP2 and PIP3 in Lipid Bilayers: Determination of Ring Orientation, And the Effects of Surface Roughness on a Poisson-Boltzmann Description. *Biophys. J.* **2009**, *97* (1), 155–63.
- (20) Jo, S.; Kim, T.; Im, W. Automated Builder and Database of Protein/Membrane Complexes for Molecular Dynamics Simulations. *PLoS One* **2007**, *2* (9), e880.
- (21) Jo, S.; Lim, J. B.; Klauda, J. B.; Im, W. CHARMM-GUI Membrane Builder for Mixed Bilayers and Its Application to Yeast Membranes. *Biophys. J.* **2009**, *97* (1), 50–58.
- (22) Jo, S.; Kim, T.; Iyer, V. G.; Im, W. CHARMM-GUI: a Web-Based Graphical User Interface for CHARMM. *J. Comput. Chem.* **2008**, *29* (11), 1859–65.
- (23) Brooks, B. R.; Brooks, C. L.; Mackerell, A. D., Jr.; Nilsson, L.; Petrella, R. J.; Roux, B.; Won, Y.; Archontis, G.; Bartels, C.; Boresch, S.; et al. CHARMM: The Biomolecular Simulation Program. *J. Comput. Chem.* **2009**, *30* (10), 1545–1614.
- (24) Klauda, J. B.; Venable, R. M.; Freites, J. A.; O'Connor, J. W.; Tobias, D. J.; Mondragon-Ramirez, C.; Vorobyov, I.; MacKerell, A. D., Jr.; Pastor, R. W. Update of the CHARMM All-Atom Additive Force Field for Lipids: Validation on Six Lipid Types. *J. Phys. Chem. B* **2010**, *114* (23), 7830–7843.
- (25) Jorgensen, W. L.; Chandrasekhar, J.; Madura, J. D.; Impey, R. W.; Klein, M. L. Comparison of Simple Potential Functions for Simulating Liquid Water. *J. Chem. Phys.* **1983**, *79* (2), 926–935.
- (26) Durell, S. R.; Brooks, B. R.; Bennaim, A. Solvent-Induced Forces between 2 Hydrophilic Groups. *J. Phys. Chem.* **1994**, *98* (8), 2198–2202.
- (27) Phillips, J. C.; Braun, R.; Wang, W.; Gumbart, J.; Tajkhorshid, E.; Villa, E.; Chipot, C.; Skeel, R. D.; Kale, L.; Schulten, K. Scalable Molecular Dynamics with NAMD. *J. Comput. Chem.* **2005**, *26* (16), 1781–1802.
- (28) Ryckaert, J. P.; Ciccotti, G.; Berendsen, H. J. C. Numerical-Integration of Cartesian Equations of Motion of a System with Constraints - Molecular-Dynamics of N-Alkanes. *J. Comput. Phys.* **1977**, *23* (3), 327–341.
- (29) Steinbach, P. J.; Brooks, B. R. New Spherical-Cutoff Methods for Long-Range Forces in Macromolecular Simulation. *J. Comput. Chem.* **1994**, *15* (7), 667–683.
- (30) Essmann, U.; Perera, L.; Berkowitz, M. L.; Darden, T.; Lee, H.; Pedersen, L. G.; Smooth, A. Particle Mesh Ewald Method. *J. Chem. Phys.* **1995**, *103* (19), 8577–8593.
- (31) Hoover, W. G. Canonical Dynamics - Equilibrium Phase-Space Distributions. *Phys. Rev. A* **1985**, *31* (3), 1695–1697.

- (32) Nose, S.; Klein, M. L. A Study of Solid and Liquid Carbon Tetrafluoride Using the Constant Pressure Molecular-Dynamics Technique. *J. Chem. Phys.* **1983**, *78* (11), 6928–6939.
- (33) Andersen, H. C. Molecular-Dynamics Simulations at Constant Pressure and/or Temperature. *J. Chem. Phys.* **1980**, *72* (4), 2384–2393.
- (34) Feller, S. E.; Zhang, Y. H.; Pastor, R. W.; Brooks, B. R. Constant-Pressure Molecular-Dynamics Simulation - the Langevin Piston Method. *J. Chem. Phys.* **1995**, *103* (11), 4613–4621.
- (35) Martyna, G. J.; Tobias, D. J.; Klein, M. L. Constant-Pressure Molecular-Dynamics Algorithms. *J. Chem. Phys.* **1994**, *101* (5), 4177–4189.
- (36) Qi, Y. F.; Im, W. Quantification of Drive-Response Relationships Between Residues During Protein Folding. *J. Chem. Theory Comput.* **2013**, *9* (8), 3799–3805.
- (37) Schreiber, T. Measuring Information Transfer. *Phys. Rev. Lett.* **2000**, *85* (2), 461–464.
- (38) Pandit, S. A.; Vasudevan, S.; Chiu, S. W.; Mashl, R. J.; Jakobsson, E.; Scott, H. L. Sphingomyelin-Cholesterol Domains in Phospholipid Membranes: Atomistic Simulation. *Biophys. J.* **2004**, *87* (2), 1092–1100.
- (39) Nagle, J. F.; Tristram-Nagle, S. Structure of Lipid Bilayers. *Biochim. Biophys. Acta* **2000**, *1469* (3), 159–195.
- (40) Kucerka, N.; Nagle, J. F.; Sachs, J. N.; Feller, S. E.; Pencer, J.; Jackson, A.; Katsaras, J. Lipid Bilayer Structure Determined by the Simultaneous Analysis of Neutron and X-Ray Scattering Data. *Biophys. J.* **2008**, *95* (5), 2356–2367.
- (41) Kim, T.; Lee, K. I.; Morris, P.; Pastor, R. W.; Andersen, O. S.; Im, W. Influence of Hydrophobic Mismatch on Structures and Dynamics of Gramicidin A and Lipid Bilayers. *Biophys. J.* **2012**, *102* (7), 1551–1560.
- (42) Vermeer, L. S.; de Groot, B. L.; Reat, V.; Milon, A.; Czaplicki, J. Acyl Chain Order Parameter Profiles in Phospholipid Bilayers: Computation from Molecular Dynamics Simulations and Comparison with H-2 NMR Experiments. *Eur. Biophys. J. Biophys.* **2007**, *36* (8), 919–931.
- (43) Lim, J. B.; Rogaski, B.; Klauda, J. B. Update of the Cholesterol Force Field Parameters in CHARMM. *J. Phys. Chem. B* **2012**, *116* (1), 203–210.
- (44) Cournia, Z.; Ullmann, G. M.; Smith, J. C. Differential Effects of Cholesterol, Ergosterol and Lanosterol on a Dipalmitoyl Phosphatidylcholine Membrane: A Molecular Dynamics Simulation Study. *J. Phys. Chem. B* **2007**, *111* (7), 1786–1801.
- (45) Shaikh, S. R.; Cherezov, V.; Caffrey, M.; Soni, S. P.; LoCascio, D.; Stillwell, W.; Wassall, S. R. Molecular Organization of Cholesterol in Unsaturated Phosphatidylethanolamines: X-Ray Diffraction and Solid State H-2 NMR Reveal Differences with Phosphatidylcholines. *J. Am. Chem. Soc.* **2006**, *128* (16), 5375–5383.
- (46) Rui, H. A.; Im, W. Protegrin-1 Orientation and Physicochemical Properties in Membrane Bilayers Studied by Potential of Mean Force Calculations. *J. Comput. Chem.* **2010**, *31* (16), 2859–2867.
- (47) Rui, H.; Im, W. Protegrin-1 Orientation in Membrane Bilayers: Insights from Potential of Mean Force Calculations as A Function of Its Tilt and Rotation Angles. *Biophys. J.* **2010**, *98* (3), 218A–218A.
- (48) Kim, T.; Jo, S.; Im, W. Solid-State NMR Ensemble Dynamics as a Mediator between Experiment and Simulation. *Biophys. J.* **2011**, *100* (12), 2922–2928.
- (49) Jo, S.; Im, W. Transmembrane Helix Orientation and Dynamics: Insights from Ensemble Dynamics with Solid-State NMR Observables. *Biophys. J.* **2011**, *100* (12), 2913–2921.
- (50) Corbin, J. A.; Dirkx, R. A.; Falke, J. J. GRP1 Pleckstrin Homology Domain: Activation Parameters and Novel Search Mechanism for Rare Target Lipid. *Biochemistry-US* **2004**, *43* (51), 16161–16173.
- (51) Psachoulia, E.; Sansom, M. S. Interactions of the Pleckstrin Homology Domain with Phosphatidylinositol Phosphate and Membranes: Characterization via Molecular Dynamics Simulations. *Biochemistry-US* **2008**, *47* (14), 4211–20.
- (52) Attree, O.; Olivos, I. M.; Okabe, I.; Bailey, L. C.; Nelson, D. L.; Lewis, R. A.; McInnes, R. R.; Nussbaum, R. L. The Lowe's Oculocerebrorenal Syndrome Gene Encodes a Protein Highly Homologous to Inositol Polyphosphate-5-Phosphatase. *Nature* **1992**, *358* (6383), 239–42.
- (53) Baraldi, E.; Djinovic Carugo, K.; Hyvonen, M.; Surdo, P. L.; Riley, A. M.; Potter, B. V.; O'Brien, R.; Ladbury, J. E.; Saraste, M. Structure of the PH Domain from Bruton's Tyrosine Kinase in Complex with Inositol 1,3,4,5-Tetrakisphosphate. *Structure* **1999**, *7* (4), 449–60.
- (54) Clement, S.; Krause, U.; Desmedt, F.; Tanti, J. F.; Behrends, J.; Pesesse, X.; Sasaki, T.; Penninger, J.; Doherty, M.; Malaisse, W.; et al. The Lipid Phosphatase SHIP2 Controls Insulin Sensitivity. *Nature* **2001**, *409* (6816), 92–7.
- (55) Kanai, F.; Liu, H.; Field, S. J.; Akbary, H.; Matsuo, T.; Brown, G. E.; Cantley, L. C.; Yaffe, M. B. The PX Domains of p47phox and p40phox Bind to Lipid Products of PI(3)K. *Nat. Cell Biol.* **2001**, *3* (7), 675–8.